

Search for events in XENON1T associated with Gravitational Waves

E. Aprile,¹ K. Abe,² S. Ahmed Maouloud,³ L. Althueser,⁴ B. Andrieu,³ E. Angelino,⁵ J. R. Angevaare,⁶ V. C. Antochi,⁷ D. Antón Martin,⁸ F. Arneodo,⁹ L. Baudis,¹⁰ A. L. Baxter,¹¹ M. Bazyk,¹² L. Bellagamba,¹³ R. Biondi,¹⁴ A. Bismark,¹⁰ E. J. Brookes,⁶ A. Brown,¹⁵ S. Bruenner,⁶ G. Bruno,¹² R. Budnik,¹⁶ T. K. Bui,² C. Cai,¹⁷ J. M. R. Cardoso,¹⁸ A. P. Cimental Chavez,¹⁰ A. P. Colijn,⁶ J. Conrad,⁷ J. J. Cuenca-García,¹⁰ V. D'Andrea,¹⁹ * M. P. Decowski,⁶ P. Di Gangi,¹³ S. Diglio,¹² K. Eitel,²⁰ A. Elykov,²⁰ S. Farrell,²¹ A. D. Ferella,^{22,19} C. Ferrari,¹⁹ H. Fischer,¹⁵ M. Flierman,⁶ W. Fulgione,^{5,19} C. Fuselli,⁶ P. Gaemers,⁶ R. Gaior,³ A. Gallo Rosso,⁷ M. Galloway,¹⁰ F. Gao,¹⁷ R. Glade-Beucke,¹⁵ L. Grandi,⁸ J. Grigat,¹⁵ H. Guan,¹¹ M. Guida,¹⁴ R. Hammann,¹⁴ A. Higuera,²¹ C. Hils,²³ L. Hoetzsche,¹⁴ N. F. Hood,²⁴ J. Howlett,¹ M. Iacobacci,²⁵ Y. Itow,²⁶ J. Jakob,⁴ F. Joerg,¹⁴ A. Joy,⁷ M. Kara,²⁰ P. Kavrigin,¹⁶ S. Kazama,²⁶ M. Kobayashi,²⁶ G. Koltman,¹⁶ A. Kopec,²⁴ F. Kuger,¹⁵ H. Landsman,¹⁶ R. F. Lang,¹¹ D. G. Layos Carlos,³ L. Levinson,¹⁶ I. Li,²¹ S. Li,¹¹ S. Liang,²¹ S. Lindemann,¹⁵ M. Lindner,¹⁴ K. Liu,¹⁷ J. Loizeau,¹² F. Lombardi,²³ J. Long,⁸ J. A. M. Lopes,¹⁸, † Y. Ma,²⁴ C. Macolino,^{22,19} J. Mahlstedt,⁷ A. Mancuso,¹³ L. Manenti,⁹ F. Marignetti,²⁵ T. Marrodán Undagoitia,¹⁴ K. Martens,² J. Masbou,¹² D. Masson,¹⁵ E. Masson,³ S. Mastroianni,²⁵ M. Messina,¹⁹ K. Miuchi,²⁷ A. Molinario,⁵ S. Moriyama,² K. Morå,¹ Y. Mosbacher,¹⁶ M. Murra,¹ J. Müller,¹⁵ K. Ni,²⁴ U. Oberlack,²³ B. Paetsch,¹⁶ J. Palacio,¹⁴ Q. Pellegrini,³ R. Peres,¹⁰ C. Peters,²¹ J. Pienaar,⁸ M. Pierre,⁶ G. Plante,¹ T. R. Pollmann,⁶ J. Qi,²⁴ J. Qin,¹¹ D. Ramírez García,¹⁰ J. Shi,¹⁷ R. Singh,¹¹ L. Sanchez,²¹ J. M. F. dos Santos,¹⁸ I. Sarnoff,⁹ G. Sartorelli,¹³ J. Schreiner,¹⁴ D. Schulte,⁴ P. Schulte,⁴ H. Schulze Eißing,⁴ M. Schumann,¹⁵ L. Scotto Lavina,³ M. Selvi,¹³ F. Semeria,¹³ P. Shagin,²³ S. Shi,¹ E. Shockley,²⁴ M. Silva,¹⁸ H. Simgen,¹⁴ A. Takeda,² P.-L. Tan,⁷ A. Terliuk,¹⁴, † D. Thers,¹² F. Toschi,²⁰ G. Trinchero,⁵ C. Tunnell,²¹ F. Tönnies,¹⁵ K. Valerius,²⁰ G. Volta,¹⁰ C. Weinheimer,⁴ M. Weiss,¹⁶ D. Wenz,²³ C. Wittweg,¹⁰ T. Wolf,¹⁴ V. H. S. Wu,²⁰ Y. Xing,¹² D. Xu,¹ Z. Xu,¹ M. Yamashita,² L. Yang,²⁴ J. Ye,¹ L. Yuan,⁸ G. Zavattini,²⁸ M. Zhong,²⁴ and T. Zhu¹
(XENON Collaboration)[§]

¹ Physics Department, Columbia University, New York, NY 10027, USA

² Kamioka Observatory, Institute for Cosmic Ray Research, and Kavli Institute for the Physics and Mathematics of the Universe (WPI), University of Tokyo, Higashi-Mozumi, Kamioka, Hida, Gifu 506-1205, Japan

³ LPNHE, Sorbonne Université, CNRS/IN2P3, 75005 Paris, France

⁴ Institut für Kernphysik, Westfälische Wilhelms-Universität Münster, 48149 Münster, Germany

⁵ INAF-Astrophysical Observatory of Torino, Department of Physics, University of Torino and INFN-Torino, 10125 Torino, Italy

⁶ Nikhef and the University of Amsterdam, Science Park, 1098XG Amsterdam, Netherlands

⁷ Oskar Klein Centre, Department of Physics, Stockholm University, AlbaNova, Stockholm SE-10691, Sweden

⁸ Department of Physics & Kavli Institute for Cosmological Physics, University of Chicago, Chicago, IL 60637, USA

⁹ New York University Abu Dhabi - Center for Astro, Particle and Planetary Physics, Abu Dhabi, United Arab Emirates

¹⁰ Physik-Institut, University of Zürich, 8057 Zürich, Switzerland

¹¹ Department of Physics and Astronomy, Purdue University, West Lafayette, IN 47907, USA

¹² SUBATECH, IMT Atlantique, CNRS/IN2P3, Université de Nantes, Nantes 44307, France

¹³ Department of Physics and Astronomy, University of Bologna and INFN-Bologna, 40126 Bologna, Italy

¹⁴ Max-Planck-Institut für Kernphysik, 69117 Heidelberg, Germany

¹⁵ Physikalisches Institut, Universität Freiburg, 79104 Freiburg, Germany

¹⁶ Department of Particle Physics and Astrophysics, Weizmann Institute of Science, Rehovot 7610001, Israel

¹⁷ Department of Physics & Center for High Energy Physics, Tsinghua University, Beijing 100084, China

¹⁸ LIBPhys, Department of Physics, University of Coimbra, 3004-516 Coimbra, Portugal

¹⁹ INFN-Laboratori Nazionali del Gran Sasso and Gran Sasso Science Institute, 67100 L'Aquila, Italy

²⁰ Institute for Astroparticle Physics, Karlsruhe Institute of Technology, 76021 Karlsruhe, Germany

²¹ Department of Physics and Astronomy, Rice University, Houston, TX 77005, USA

²² Department of Physics and Chemistry, University of L'Aquila, 67100 L'Aquila, Italy

²³ Institut für Physik & Exzellenzcluster PRISMA⁺, Johannes Gutenberg-Universität Mainz, 55099 Mainz, Germany

²⁴ Department of Physics, University of California San Diego, La Jolla, CA 92093, USA

²⁵ Department of Physics “Ettore Pancini”, University of Napoli and INFN-Napoli, 80126 Napoli, Italy

²⁶ Kobayashi-Maskawa Institute for the Origin of Particles and the Universe, and Institute for Space-Earth Environmental Research, Nagoya University, Furo-cho, Chikusa-ku, Nagoya, Aichi 464-8602, Japan

²⁷ Department of Physics, Kobe University, Kobe, Hyogo 657-8501, Japan

²⁸ INFN - Ferrara and Dip. di Fisica e Scienze della Terra, Università di Ferrara, 44122 Ferrara, Italy

(Dated: June 22, 2023)

We perform a blind search for particle signals in the XENON1T dark matter detector that occur close in time to gravitational wave signals in the LIGO and Virgo observatories. No particle signal is

observed in the nuclear recoil, electronic recoil, $\text{CE}\nu\text{NS}$, and S2-only channels within ± 500 seconds of observations of the gravitational wave signals GW170104, GW170729, GW170817, GW170818, and GW170823. We use this null result to constrain mono-energetic neutrinos and Beyond Standard Model particles emitted in the closest coalescence GW170817, a binary neutron star merger. We set new upper limits on the fluence (time-integrated flux) of coincident neutrinos down to 17 keV at 90% confidence level. Furthermore, we constrain the product of coincident fluence and cross section of Beyond Standard Model particles to be less than $10^{-29} \text{ cm}^2/\text{cm}^2$ in the [5.5–210] keV energy range at 90% confidence level.

Keywords: Dark Matter, Direct Detection, Xenon

I. INTRODUCTION

Following the first detection of a gravitational wave (GW) signal by the Laser Interferometer Gravitational-Wave Observatory (LIGO) in 2016 [1], GW signals from binary mergers are now routinely detected by the LIGO and Virgo observatories [2]. The subsequent observation of electromagnetic counterparts from binary neutron star coalescence in 2017 [3] has made GW signals an integral part of multi-messenger astrophysics. Various detectors have conducted follow-up searches for neutrinos associated with binary mergers in a time window of $\pm [400\text{--}500]\text{ s}$ of the observed GW signal [4–10], which might indicate the simultaneous emission of relativistic particles. The sensitive (neutrino) energy ranges of these searches, summarized in Tab. I, span from EeV down to half an MeV. No evidence of a particle signal, coincident with GW signal, has been reported yet. Here, we use data from the XENON1T dark matter search [11] to extend this neutrino energy window down to 17 keV. Further, the low threshold of 1 keV electron-equivalent (keV_{ee}) offered by the XENON1T, enables us to search for Beyond Standard Model (BSM) particles from the merger of neutron stars, such as relativistic axions [12, 13] or sterile neutrinos [14, 15].

TABLE I. Search for particles coincident with GW and the energy ranges they are sensitive to.

Detector	Detection energy
Pierre Auger Observatory [4]	$10^{11} \text{ MeV} - 10^{13} \text{ MeV}$
IceCube [5]	$10^5 \text{ MeV} - 10^{11} \text{ MeV}$
Super-K [6]	$3.5 \text{ MeV} - 10^{11} \text{ MeV}$
XMASS [7]	$14 \text{ MeV} - 100 \text{ MeV}$
KamLAND [8]	$1.8 \text{ MeV} - 111 \text{ MeV}$
NOvA [9]	$1 \text{ MeV} - 10 \text{ MeV}$
Borexino [10]	$0.5 \text{ MeV} - 5 \text{ MeV}$
XENON1T (this work)	$0.017 \text{ MeV} - 50 \text{ MeV}$

II. DATA SETS

The LIGO and Virgo observatories conducted their second observation run from November 30, 2016, to August 25, 2017 [21]. Overlapping with this time frame, the XENON1T detector took Science Run 0 (SR0) data from November 22, 2016 to January 18, 2017, and Science Run 1 (SR1) data from February 2, 2017 to February 8, 2018. This data has already been analyzed in several channels that we revisit here in order to check for particle signals coincident with LIGO and Virgo GW observations.

The XENON1T experiment has been described in [11]. A search for nuclear recoils (NR) demanding both scintillation light (S1) and electroluminescence from ionization electrons (S2) is available during both SR0 [16] and SR1 [17]. In addition, using data from SR1, a search was conducted for electronic recoils (ER) [18], for nuclear recoils produced by solar neutrinos via coherent elastic neutrino-nucleus scattering ($\text{CE}\nu\text{NS}$) [19], and for nuclear recoils where the requirement of a scintillation signal has been waived (S2-only) [20]. Details of these analysis channels can be found in the respective papers [16–20]. Notably, the NR and ER channels demand coincident signals from at least three photomultiplier tubes (PMTs) for an S1, while the $\text{CE}\nu\text{NS}$ channel requires signals from only two PMTs. Furthermore, the S2 threshold has been reduced from 200 photoelectrons (PE) and 500 PE for the NR and ER channels, respectively, to 120 PE and 150 PE for the $\text{CE}\nu\text{NS}$ and S2-only channels, respectively.

The corresponding energy ranges of these channels are given in Tab. II in units of keV electron-equivalent (keV_{ee}) for the ER channel, and as keV nuclear recoil-equivalent (keV_{nr}) for the NR, $\text{CE}\nu\text{NS}$, and S2-only channels. Effective xenon target masses vary for different analyses. Whereas the exposure of the NR, ER, and $\text{CE}\nu\text{NS}$ channels is limited by the fiducial volume, the S2-only channel is limited by the strong event selections applied to reduce backgrounds.

The background rate is very low for the NR, $\text{CE}\nu\text{NS}$, and S2-only channels (see Tab. II), which motivates the use of a single energy bin for each of these channels. However, the background rate is quite high in ER channel due to the β decay of ^{214}Pb , present due to ^{222}Rn emanation by materials [18]. Further, from Fig. 3 of [18], we can see that the ER spectrum is not constant in energy. The spectrum exhibits spectral lines from radioactive ^{83m}Kr and ^{131m}Xe . We thus define five energy bins for the ER

* Also at INFN - Roma Tre, 00146 Roma, Italy

† Also at Coimbra Polytechnic - ISEC, 3030-199 Coimbra, Portugal

‡ Also at Physikalisches Institut, Universität Heidelberg, Heidelberg, Germany

§ rriya@purdue.edu

TABLE II. Characteristics of analysis channels considered in this study. For each of these channels, we show the corresponding energy ranges, the Science Runs that have been analyzed for that channel, the fiducial target mass, and the observed background rate. Further, in the ± 500 s time window around a GW event, we give the average livetime for detecting a signal, the average number of expected background events (N_{exp}), and the probability of observing zero background events ($P(0)$).

Event channel	Energy range	Runs analyzed	Fiducial target mass	Background rate (events/day)	Livetime (per GW)	N_{exp}	$P(0)$
NR [16, 17]	4.9 keV _{nr} – 40.9 keV _{nr}	SR0, SR1	1.3 tonne	0.05	935 s	0.00054	0.9995
ER [18]	1 keV _{ee} – 210 keV _{ee}	SR1	1.04 tonne	186	935 s	See Tab. IV	See Tab. IV
CE ν NS [19]	≥ 1.6 keV _{nr}	SR1	1.04 tonne	0.03	790 s	0.00027	0.9997
S2-only [20]	≥ 0.7 keV _{nr}	SR1	0.12 tonne	0.94	650 s	0.0071	0.993

channel: low energy (0–30 keV_{ee}), ^{83m}Kr (30–50 keV_{ee}), medium energy (50–142 keV_{ee}), ^{131m}Xe (142–185 keV_{ee}) and high energy (185–210 keV_{ee}).

Three of the eight GW signals that LIGO/VIRGO observed during SR0 and SR1 occurred during XENON1T calibration or downtime. Only SR0 NR data is available during GW170104, while SR1 data in all four analysis channels is available during GW170729, GW170817, GW170818, and GW170823. Out of these, GW170817 was due to the merger of neutron stars, and was at a distance of 40 Mpc, compared to a distance of ~ 1000 Mpc for other events. Out of these GWs, the particle flux is dominated by GW170817 because the flux is inversely proportional to the square of distance.

III. NEUTRINO SPECTRA

Neutrinos predominantly interact in our detector via elastic scattering off electrons or xenon nuclei. The standard model differential cross section for elastic neutrino-electron scattering can be written as [22, 23],

$$\frac{d\sigma_{\text{ES}}}{dE_r} = \frac{G_F^2 m_e}{2\pi} \left[(g_V + g_A)^2 - (g_V^2 - g_A^2) \frac{m_e E_r}{E_\nu^2} \right. \\ \left. + (g_V - g_A)^2 \left(1 - \frac{E_r}{E_\nu} \right)^2 \right],$$

where E_r is the electron recoil kinetic energy, E_ν is the incoming neutrino energy, m_e is the mass of an electron, and G_F is the Fermi constant. Neutrino-electron coupling constants for different flavors of neutrinos and antineutrinos are furnished in Tab. III.

The expected number of signals in the ER channel is given as,

$$\frac{dN_{\text{ER}}}{dE_r} = N_T(E_r) \epsilon(E_r) \int \frac{d\sigma_{\text{ES}}}{dE_r} \frac{df(E_\nu)}{dE_\nu} dE_\nu, \quad (1)$$

where $\epsilon(E_r)$ is the detection efficiency of the ER channel as a function of the recoil energy [18]. $f(E_\nu)$ is the neutrino energy spectrum. $N_T(E_r)$ is the total number of available electrons in the fiducial target: $N_T(E_r) = N_{\text{Xe}} \times N_e$, where N_{Xe} is the total number of xenon atoms

TABLE III. Neutrino-electron coupling constants for different flavors of neutrinos and antineutrinos. θ_W is the Weinberg angle.

Neutrino flavor	g_V	g_A
ν_e	$2 \sin^2 \theta_W + \frac{1}{2}$	$+\frac{1}{2}$
$\bar{\nu}_e$	$2 \sin^2 \theta_W + \frac{1}{2}$	$-\frac{1}{2}$
ν_μ, ν_τ	$2 \sin^2 \theta_W - \frac{1}{2}$	$-\frac{1}{2}$
$\bar{\nu}_\mu, \bar{\nu}_\tau$	$2 \sin^2 \theta_W - \frac{1}{2}$	$+\frac{1}{2}$

in the fiducial volume and N_e is number of electrons per xenon atom with binding energies below the particular recoil energy. The different shells of a xenon atom, along with the number of electrons and the potential energy, are given in [24].

The effective cross section as a function of neutrino energy, taking into account the detector properties, is shown in Fig. 1 (left). We use the free electron approximation because a more precise relativistic random phase approximation is unavailable for our energy region of interest. We convolve the cross section with a Gaussian function with standard deviation $0.31\sqrt{E \text{ keV}} + 0.0037E$ [18] to account for energy resolution, where E is in keV. We also account for the fact that a neutrino can not produce a recoil of energy greater than $2E_\nu^2/(2E_\nu + m_e)$ [23]. Our threshold of 1 keV_{ee} makes us insensitive to neutrinos of energy 16 keV or below. Given an absence of theoretical predictions, we assume that neutrinos are emitted mono-energetically in binary mergers, as done in previous low-energy searches [6, 7, 10]. The cross section for electronic recoils depends weakly on neutrino energy, it is almost constant at neutrino energies above 36 keV. However, it decreases below 36 keV because low-energy neutrinos are incapable of generating electronic recoils throughout the entire energy range of ER channel (1 keV_{ee} – 210 keV_{ee}).

Having discussed the interaction of neutrinos with electrons, we now turn to the interaction of neutrinos with xenon nuclei. Neutrinos in the energy range of 10 – 50 MeV can interact coherently with nuclei [25]. For CE ν NS, we use the same differential cross section as

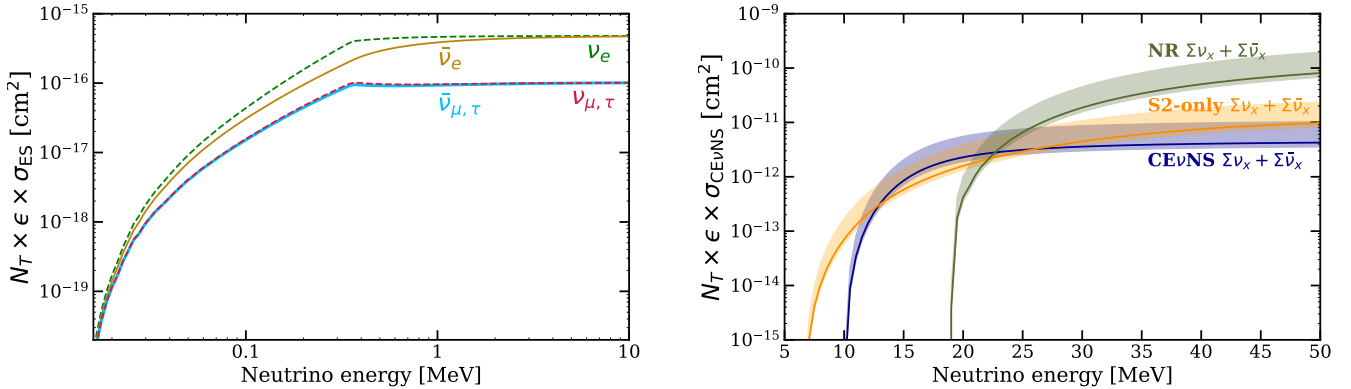


FIG. 1. Left: the effective cross section for elastic neutrino-electron scattering as a function of neutrino energy for electron neutrinos (ν_e , dashed green), electron antineutrinos ($\bar{\nu}_e$, solid gold), muon or tau neutrinos ($\nu_{\mu,\tau}$, dashed red), and muon or tau antineutrinos ($\bar{\nu}_{\mu,\tau}$, solid cyan). Right: the effective cross section for $\text{CE}\nu\text{NS}$ as a function of neutrino energy. NR (olive-green), $\text{CE}\nu\text{NS}$ (blue), and S2-only (orange) refer to different ways in which the data was analyzed in the search for nuclear recoils, as described in Sec. II. In the right plot, the cross section is for the interaction of all flavors of neutrinos and antineutrinos.

in [19]. The number of nuclear recoils in the detector has a similar form as Eq. (1), with $N_T(E_r)$ and σ_{ES} replaced by N_{Xe} and $\sigma_{\text{CE}\nu\text{NS}}$ respectively. Also, $\epsilon(E_r)$ is the detection efficiency of considered channels as a function of the nuclear recoil kinetic energy. Assuming mono-energetic emission of the neutrinos, the effective cross section as a function of neutrino energy, taking into account the detector properties, is shown in Fig. 1 (right). We also consider non-standard neutrino interactions via the vector coupling of ν_e to up and down quarks. The coupling values within 90% confidence interval from XENON1T data [19], can effectively change the total interaction cross section from a factor of 0.83 to 2.42, under the assumption that 1/6th of the total neutrinos are electron neutrinos. The resulting changes in the number of nuclear recoils are shown as an uncertainty band.

IV. BACKGROUND ESTIMATION

Consistent with previous coincidence searches shown in Tab. I, which used a time window of $\pm [400\text{--}500]\text{ s}$, we use a $\pm 500\text{ s}$ time window centered on the time of GW signal. This is appropriate for any relativistic particle flux emitted by the binary merger. Accounting for deadtime due to various cuts and background events, livetimes for detecting a signal in the $\pm 500\text{ s}$ time window around a GW signal in the NR, ER, $\text{CE}\nu\text{NS}$ and S2-only channels are approximately 935 s, 935 s, 790 s and 650 s respectively.

Although background events in these channels have been studied before, a direct comparison with the timing of gravitational waves has never been made. To ensure an unbiased analysis, we follow a blind approach where we refrain from utilizing the timing information of individual background events until the background model is finalized and the expected number of background events

in the $\pm 500\text{ s}$ time window is determined.

Fig. 2 shows the distribution of background events with time in different analysis channels. Rates are constant within statistical uncertainty for the duration of the Science Runs for the NR, $\text{CE}\nu\text{NS}$, and S2-only channels. Therefore, for these channels, the background rate is the ratio of the total number of background events during the entire Science Run and the total livetime of the entire Science Run.

However, due to the background of activated isotopes — $^{131\text{m}}\text{Xe}$, ^{133}Xe , and ^{125}I ; we need to account for the time-dependence of background rate. Thus, we use the same background estimation for the ER channel as in [26]. Before unblinding the timing information of background events, we compare the values predicted by these background models with the actual observations in the different energy bins. The comparison was done using the $(-1500, -500)\text{ s}$ sideband before the GW events. To account for the degree of freedom due to five independent ER energy bins and four GW signals, we divided the chi-square by 20 and found the reduced chi-square statistic to be 1.14. This confirms that these background models agree with the observation.

Table II gives background rate and livetime in the units of events/day and seconds respectively. Therefore, the expected number of background events in the $\pm 500\text{ s}$ time window around a GW signal, is calculated as,

$$N_{\text{exp}} = \text{background rate} \times \frac{\text{livetime}}{24 \times 60 \times 60}. \quad (2)$$

The corresponding probabilities of observing zero background events are values of cumulative distribution functions at zero, assuming Poisson statistics. These values are given in Tab. II for the NR, $\text{CE}\nu\text{NS}$, and S2-only channels and in Tab. IV for the ER channel.

The $\pm 500\text{ s}$ time window was blinded during background estimation, and we calculated the upper limit on

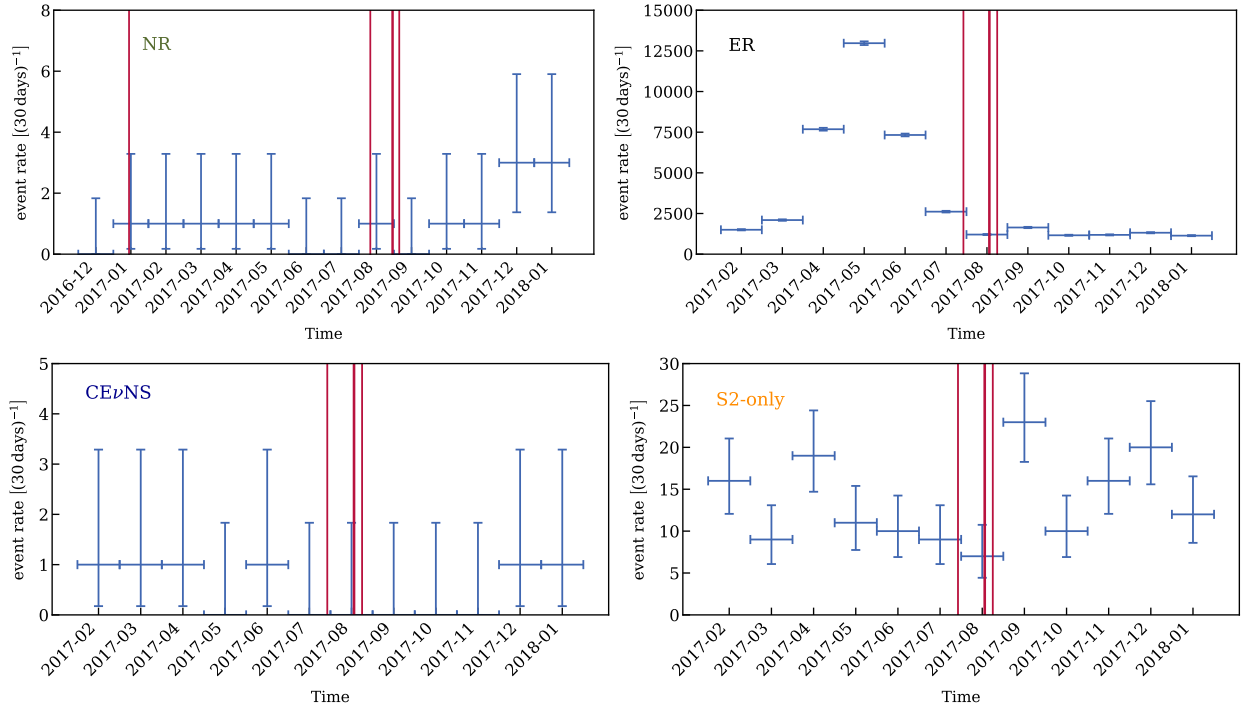


FIG. 2. The distribution of background events with time in different analysis channels. Red lines indicate the time of GW events. The rise and subsequent decay of event rate in the ER channel during March-September are due to production of ^{131m}Xe , ^{133}Xe , and ^{125}I during neutron calibration campaigns [26].

TABLE IV. Predictions for the different energy bins of the ER channel during four GW events. For each bin, in the ± 500 s time window around a GW event, we give the number of expected background events (N_{exp}), the probability of observing zero background events ($P(0)$) and the upper limits (UL) on the expected number of background events at a 3σ confidence level.

	Low Energy			^{83m}Kr			Medium Energy			^{131m}Xe			High Energy		
	N_{exp}	$P(0)$	UL	N_{exp}	$P(0)$	UL	N_{exp}	$P(0)$	UL	N_{exp}	$P(0)$	UL	N_{exp}	$P(0)$	UL
GW170729	0.04	0.94	2	0.16	0.85	3	0.22	0.80	3	0.64	0.52	5	0.07	0.93	2
GW170817	0.04	0.94	2	0.15	0.86	3	0.22	0.80	3	0.29	0.75	4	0.07	0.93	2
GW170818	0.04	0.94	2	0.15	0.86	3	0.22	0.80	3	0.27	0.76	4	0.07	0.93	2
GW170823	0.04	0.94	2	0.14	0.87	3	0.22	0.80	3	0.23	0.79	3	0.07	0.93	2

the expected number of background events in the ER channel, based on the background model, above which evidence for a particle signal could have been claimed. For Poisson statistics, the relationship between local p-value and global p-value taking into account 20 degrees of freedom (n_{dof}) is given by Sidak Correction [27],

$$P_{\text{global}} = 1 - (1 - p_{\text{local}})^{1/n_{\text{dof}}}. \quad (3)$$

The local p-value of 3×10^{-3} corresponds to a global p-value of 1.5×10^{-4} for a potential excess at a 3σ confidence level. The resulting upper limits on the expected number of background events are between 2 and 5, as shown in Tab. IV. We do not give upper limits on the expected number of background events in the other channels because values of cumulative distribution functions at 1, for Poisson distributions with such small means, are more than 99.99%.

V. RESULTS AND CONCLUSIONS

Once these detection channels, time and energy ranges, and background models were fixed, the timing information of background events was unblinded. No background event was observed in any of these channels within ± 500 seconds of any tested GW signal. Given the low background rates, this is expected under the background-only hypothesis in the NR, CE ν NS, and S2-only channels. The total number of expected background events in all energy bins of the ER channel across all GWs is ~ 3 . However, even in this channel, no background events were observed, consistent with the background-only hypothesis, assuming Poisson statistics, within a 3σ confidence interval.

The absence of background events can be converted into an upper limit on coincident neutrinos emitted in

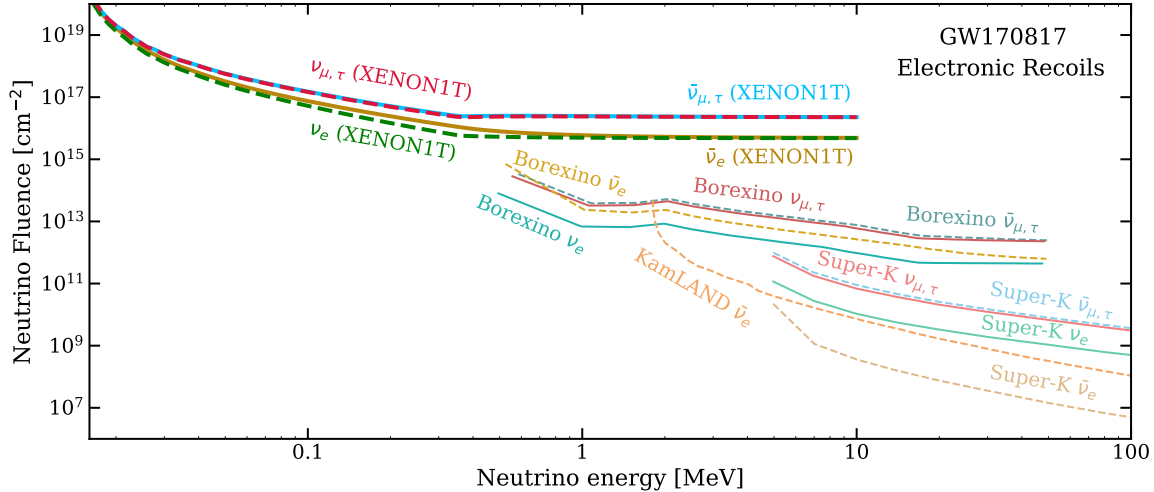


FIG. 3. The upper limit on the fluence (time-integrated flux) of coincident neutrinos emitted in GW170817, the merger of neutron stars using the electronic recoil signals in XENON1T, obtained for electron neutrinos (ν_e , dashed green), electron antineutrinos ($\bar{\nu}_e$, solid gold), muon or tau neutrinos ($\nu_{\mu,\tau}$, dashed red), and muon or tau antineutrinos ($\bar{\nu}_{\mu,\tau}$, solid cyan). We also show the limits obtained by Borexino [10], KamLAND [8], and Super-K [6] for comparison.

the mergers, assuming a Poisson distribution of neutrino signal events [28]. To ensure consistency with other experiments, we place limits at a 90% confidence level on fluence, which represents the integration of flux with respect to time. We are most sensitive to the merger of neutron stars – GW170817, due to its close proximity [3]. The upper limit on neutrino fluence at 90% confidence level using electronic recoils is shown in Fig. 3. As can be seen, we place upper limits on the fluence of $\mathcal{O}(10)$ keV neutrinos. No other detector has been able to probe such low-energy neutrinos. The upper limit on neutrino fluence at 90% confidence level using nuclear recoils is shown in Fig. 4. Our limits are comparable to those from the XMMASS dark matter detector. Both limits are on the sum of the fluence of all flavors of neutrinos and antineutrinos, which is different for the stronger limits from Super-K.

We also use our data to constrain the fluence of BSM particles with keV energies coincident with GW events, such as axions or sterile neutrinos. Similar to neutrinos, we assume that these BSM particles are emitted mono-energetically. Further, in the absence of a concrete model for the interaction of these BSM particles with electrons, we assume that all of their energy is transferred to the electron during an interaction. For this assumption to be valid, the particles' rest mass must be negligible compared to their total energy of $\mathcal{O}(10)$ keV. These assumptions yield the number of electronic recoils in the detector due to BSM particles as,

$$N_{\text{ER}} = N_T \epsilon \sigma_{\text{BSM}} F_{E_{\text{BSM}}}, \quad (4)$$

where σ_{BSM} is the cross section of BSM particles to interact with electrons and $F_{E_{\text{BSM}}}$ is the fluence of BSM par-

ticles with energy E_{BSM} . It can be seen in Fig. 2 of [18] that the efficiency of our detector for the ER channel is $\sim 89\%$ for recoil energies greater than 5 keV_{ee}. The number of electrons available per atom when the recoil energy is greater than 34.6 (5.5) keV_{ee} is 54 (52) electrons. Given that we do not see any background event, we obtain the upper limit on the product of coincident fluence and cross section: $\sigma_{\text{BSM}} F_{E_{\text{BSM}}} < 10^{-29} \text{ cm}^2/\text{cm}^2$ for E_{BSM} in [5.5–210] keV_{ee}.

We have thus provided the first search for particle signals in the keV energy region associated with GWs. Despite the 1.3 tonnes fiducial mass of XENON1T, various recoil channels, energy regions down to 1 keV_{ee}, no particle signals were found within ± 500 s time windows around GW signals. As a result, we extended the upper limits on the coincident fluence down to neutrino energy of 17 keV. Further, we put an upper limit on the product of coincident fluence and cross section of general BSM particles interacting with atomic electrons. These limits can help constrain models involving neutrinos or other BSM particles in binary star mergers. As gravitational wave detectors will continue taking data during the operation of the current and next generation of multiple tonnes xenon detectors [29–33], future GWs from nearby mergers will further improve these constraints.

VI. ACKNOWLEDGEMENTS

We gratefully acknowledge support from the National Science Foundation, Swiss National Science Foundation, German Ministry for Education and Research, Max Planck Gesellschaft, Deutsche Forschungsgemeinschaft,

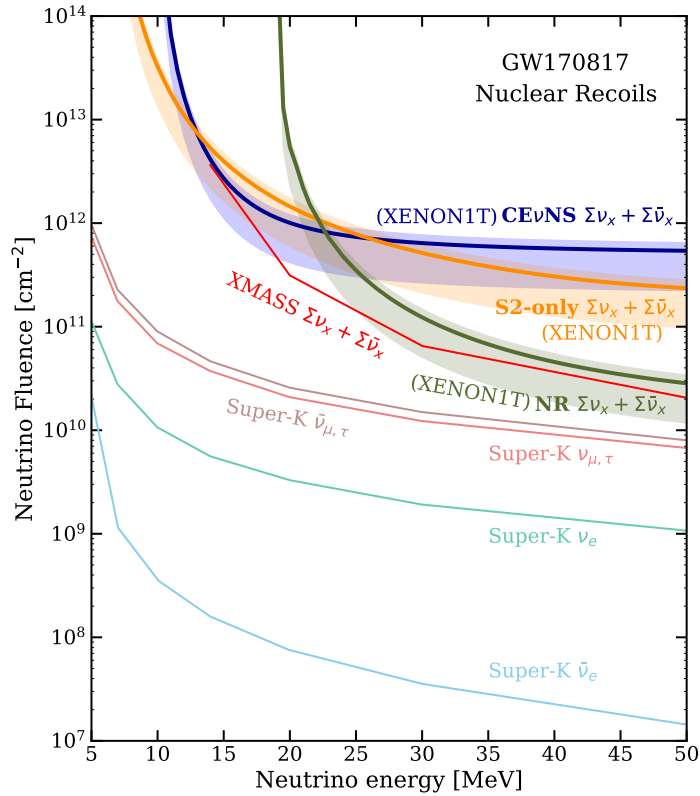


FIG. 4. The upper limit on the fluence (time-integrated flux) of coincident neutrinos emitted in GW170817, the merger of neutron stars using the nuclear recoil signals in XENON1T, placed on the sum of the fluence of all flavors of neutrinos and antineutrinos. NR (olive-green), CE ν NS (blue), and S2-only (orange) refer to different ways in which the data was analyzed in search for nuclear recoils, as described in Sec. II. We also show the limits obtained by XMASS [7] and Super-K [6] for comparison.

Helmholtz Association, Dutch Research Council (NWO), Weizmann Institute of Science, Israeli Science Foundation, Binational Science Foundation, Fundacao para a Ciencia e a Tecnologia, Région des Pays de la Loire, Knut and Alice Wallenberg Foundation, Kavli Foundation, JSPS Kakenhi and JST FOREST Program in Japan, Tsinghua University Initiative Scientific Research Program and Istituto Nazionale di Fisica Nucleare. This project

has received funding/support from the European Union’s Horizon 2020 research and innovation programme under the Marie Skłodowska-Curie grant agreement No 860881-HIDDeN. Data processing is performed using infrastructures from the Open Science Grid, the European Grid Initiative and the Dutch national e-infrastructure with the support of SURF Cooperative. We are grateful to Laboratori Nazionali del Gran Sasso for hosting and supporting the XENON project.

[1] B. P. Abbott et al. (LIGO Scientific, Virgo), Phys. Rev. Lett. **116**, 061102 (2016), 1602.03837.

[2] R. Abbott et al. (LIGO Scientific, VIRGO, KAGRA) (2023), 2302.03676.

[3] B. P. Abbott et al. (LIGO Scientific, Virgo), Phys. Rev. Lett. **119**, 161101 (2017), 1710.05832.

[4] E. Santos (Pierre Auger), J. Phys. Conf. Ser. **1181**, 012060 (2019).

[5] R. Abbasi et al. (IceCube) (2023), 2303.15970.

[6] Y. Hayato et al. (Super-Kamiokande), Astrophys. J. Lett. **857**, L4 (2018), 1802.04379.

[7] K. Abe et al. (XMASS), Astropart. Phys. **129**, 102568 (2021), 2007.16046.

- [8] S. Abe et al. (KamLAND), *Astrophys. J.* **909**, 116 (2021), 2012.12053.
- [9] M. A. Acero et al. (NOvA), *Phys. Rev. D* **101**, 112006 (2020), 2001.07240.
- [10] D. Basilico et al. (BOREXINO) (2023), 2303.13876.
- [11] E. Aprile et al. (XENON), *Eur. Phys. J. C* **77**, 881 (2017), 1708.07051.
- [12] S. P. Harris, J.-F. Fortin, K. Sinha, and M. G. Alford, *JCAP* **07**, 023 (2020), 2003.09768.
- [13] D. F. G. Fiorillo and F. Iocco, *Phys. Rev. D* **105**, 123007 (2022), 2109.10364.
- [14] M. U. Frensel, Ph.D. thesis, Basel U. (main) (2017).
- [15] M. Frensel, M.-R. Wu, C. Volpe, and A. Perego, *Phys. Rev. D* **95**, 023011 (2017), 1607.05938.
- [16] E. Aprile et al. (XENON), *Phys. Rev. Lett.* **119**, 181301 (2017), 1705.06655.
- [17] E. Aprile et al. (XENON), *Phys. Rev. Lett.* **121**, 111302 (2018), 1805.12562.
- [18] E. Aprile et al. (XENON), *Phys. Rev. D* **102**, 072004 (2020), 2006.09721.
- [19] E. Aprile et al. (XENON), *Phys. Rev. Lett.* **126**, 091301 (2021), 2012.02846.
- [20] E. Aprile et al. (XENON), *Phys. Rev. Lett.* **123**, 251801 (2019), 1907.11485.
- [21] B. P. Abbott et al. (LIGO Scientific, Virgo), *Phys. Rev. X* **9**, 031040 (2019), 1811.12907.
- [22] C. Giunti and A. Studenikin, *Phys. Atom. Nucl.* **72**, 2089 (2009), 0812.3646.
- [23] P. Vogel and J. Engel, *Phys. Rev. D* **39**, 3378 (1989).
- [24] M. Winter, *Xenon: Properties of free atoms*, URL <https://www.webelements.com/xenon/atoms.html>.
- [25] M. Abdullah et al. (2022), 2203.07361.
- [26] E. Shockley, *Study of Excess Electronic Recoil Events in Xenon1T* (2021).
- [27] Z. Šidák, *Journal of the American Statistical Association* **62**, 626 (1967).
- [28] G. J. Feldman and R. D. Cousins, *Phys. Rev. D* **57**, 3873 (1998), physics/9711021.
- [29] E. Aprile et al. (XENON) (2023), 2303.14729.
- [30] J. Aalbers et al. (LZ) (2022), 2207.03764.
- [31] J. Liu (PandaX), *Int. J. Mod. Phys. D* **31**, 2230007 (2022).
- [32] J. Aalbers et al., *J. Phys. G* **50**, 013001 (2023), 2203.02309.
- [33] XLZD, *Dark matter detection consortium*, URL <https://xlzd.org/>.